catalysts

MDPI

Article

Production of 1,3-Butadiene from Ethanol Using Treated Zr-Based Catalyst

Adama A. Bojang and Ho-Shing Wu *

Department of Chemical Engineering and Materials Science, Yuan Ze University, 135 Yuan Tung Road, Chung Li, Taoyuan 32003, Taiwan; zazafj1990@gmail.com

* Correspondence: cehswu@saturn.yzu.edu.tw; Tel.: +886-3-4638800-2564

Abstract: The conversion of ethanol to 1,3-butadiene was carried out using a treated Zr-based catalyst at a temperature of 350–400 °C with different weight hourly space velocities in a fixed bed reactor. The catalysts used are commercial, but they underwent pretreatment. The commercial catalysts used were ZrO_2, $Zr(OH)_2$, 2% CaO-ZrO_2, 30% TiO_2-ZrO_2, 50% CeO_2-ZrO_2 and 10% SiO_2-ZrO_2 in their modified or treated form. The characterizations of the catalysts were carried out using XRD, XPS, and TGA. The results indicated that ethanol conversion, yield, and selectivity of 1,3-butadiene operated weight hourly space velocity of 2.5 h^{-1} using 10% SiO_2-ZrO_2 were 95%, 80%, and 85%, respectively, at 350 °C. Using 50% CeO_2-ZrO_2 converted 70% ethanol with a 1,3-butadiene yield of 65%. The best Zr-based catalyst was 10% SiO_2-ZrO_2 as it gives a steady 1,3-butadiene yield, the Si-composition with ZrO_2 gives a good catalytic pour of the catalyst-bed structure; hence, the life span was good. Using 30% TiO_2-ZrO_2 has an ethanol conversion of 70% with a 1,3-butadiene yield of 43%.

Keywords: 1,3-butadiene; ethanol; zirconium; acetaldehyde; ethylene

Citation: Bojang, A.A.; Wu, H.-S. Production of 1,3-Butadiene from Ethanol Using Treated Zr-Based Catalyst. *Catalysts* **2022**, *12*, 766. https://doi.org/10.3390/catal12070766

Academic Editors: Sagadevan Suresh and Is Fatimah

Received: 31 May 2022
Accepted: 8 July 2022
Published: 11 July 2022

1. Introduction

The chemical 1,3-butadiene is very important in the manufacturing of isomers in rubber industries. It can be used in the large-scale production of organic chemicals in synthetic chemical reactions, e.g., the Diels–Alder reaction. Since it belongs to the lower hydrocarbon group, its production is mostly from condensation reactions in the form of cracking. Since the butadiene vintage hinges principally on the type of biomass or the reactant in the condensation cracker, butadiene fabrication is vulnerable to market unpredictability or styles in the gasoline business, notably the evolving routine of gas, which might lead to butadiene deficiencies. The insufficiency of greenhouse gas-emitting fuel reserves is another long-running issue with the present hydrocarbon production methodology, in terms of profitable and environmental property. These staples have recently revived an interest in the century-old, heterogeneous chemical process transformation of alcohol to hydrocarbon, within which vaporized alcohol is primarily reworked to hydrocarbon (butadiene).

The ethanol to butadiene production process can occur in two basic steps: one-step and two-step processes. The Lebedev process often used a one-step process, by which ethanol is processed in the gas-phase form and later is converted to butadiene [1]. The Ostromislensky process is also known as the two-step process. In this process, ethanol is in a ration with acetaldehyde in a gas phase in which the dehydrogenation of ethanol is ideal [2]. The one-step process typically favors the production of acetaldehyde with little butadiene yield. Meanwhile, acetaldehyde can be recycled in industries to produce butadiene in further reaction synthesis with a specifically designed catalyst.

Consequently, even in the one-step process, it is indispensable to test feeds containing acetaldehyde to assess the comportment of the catalytic system in acetaldehyde-containing mixtures, nevertheless, in lower quantities compared to the two-step process [3–7]. Since ancient times, humans have used sugar fermentation to produce ethanol, one of the earliest

of several biotechnologies [8]. Bioethanol made from the microbial fermentation of the biomass was changed from the sugar into ethanol and the same happens with petrochemical raw materials to produce ethanol, which can be produced from fermentation processes using renewable substrates such as glucose, starch, and others. The dehydration of ethanol can replace steam-cracking fossil fuels to produce ethylene and 1,3-butadiene [5,6,9]. In addition, with the progress of bioethanol technology and the popularization of bioethanol industrial equipment, the production of butadiene from bioethanol has become a sustainable green chemical route for the supply of butadiene.

Generally, ethanol dehydration to butadiene or ethylene is conducted using solid acidic or basic catalysts. The Zr-based catalyst was its reactivity and stability over the Mg-based catalyst since those are the catalysts in our preliminary study. Also, treating Zr with oxalic acid gives well-coordinated acidic and basic surroundings if necessary. ZrO_2, Zr/Si, and CaO/Zr-containing catalysts are usually used at a temperature of 300–425 °C, at standard pressure [10–13]. It was suggested that the catalyst activity could be correlated with the number of strong Brønsted acid sites in the catalyst. Table 1 highlights the use of Zr-containing catalyst for 1,3-butadiene production from ethanol. Modifying the Cu/Zr-Si catalyst with lanthanum increases their activity in aqueous ethanol conversion into 1,3-butadien [14]. Sushkevich et al. discuss the use of Zr-based catalyst in combination with zeolites beta catalyst which was obtained using synthetic modification methods, the result yielded a high selectivity of 1,3-butadiene (74 mol%), and the acidic nature of the catalyst was a key determinant for the general reaction synthesis [15,16].

The novelty of this study gives a general understanding of the catalytic performance of treated-Zr-based catalytic systems when using aqueous ethanol in an ethanol to butadiene process. This study examines the effect of a treated-Zr-based catalyst in the production of 1,3-butadiene. It also gives the relevant information on oxalic acid used in the treatment of each sample of the commercial catalyst [13,17]. The reason for selecting the Zr-based catalyst was its reactivity and stability over the Mg-based catalyst, since those are the catalysts at our disposal. Also, treating Zr with oxalic acid gives well-coordinated acidic and basic surroundings if necessary. This study aims to improve the catalytic activity of the commercial catalyst by treating it with oxalic acid, NaOH, and other essential acidic compounds. As the results show, the treated commercial catalyst yielded a better 1,3-butadiene production than the untreated. Also, the presence of oxalic acid in combination with NaOH will provide a good desilication process and increase the catalyst's acidic properties.

Table 1. Zr-containing catalyst for 1,3-butadiene production from ethanol.

Catalyst	T (°C)	WHSV (h^{-1})	TOS (h)	X_{EtOH} (%)	$Y_{1,3\text{-}BD}$ (%)	Refs.
4.9% Cu/MCF + 2.7% Zr/MCF	425	3.7	10	92	64.4	[18]
3.7% Ag/Zr/BEA	350	1.2–3.7	3	-	-	[15,19]
3% ZrO_2/SiO_2	350	1.8	-	45.4	31.6	[20,21]
3000 ppm $Na/Zn_1Zr_{10}O_n$	400	6.2	-	54.4	15.2	[22]
ZrO_2	350	2.5	14	50	28	This study
$Zr(OH)_2$	350	2.5	14	30	19	
2%CaO-ZrO_2	350	2.5	14	79	30	
10% SiO_2-ZrO_2	350	2.5	15	95	80	
30% TiO_2-ZrO_2	350	2.5	14	70	43	
50% CeO_2-ZrO_2	350	2.5	14	70	65	

X: ethanol conversion Y: 1,3 butadiene selectivity, WHSV: weight hourly space velocity, TOS: time on stream, T: temperature.

2. Results and Discussion

2.1. Crystalline Properties of the Catalyst

The catalytic characterizations of ZrO_2, $Zr(OH)_2$, 10% SiO_2-ZrO_2, and 2% CaO-ZrO_2 using XRD are shown in Figure 1. For ZrO_2, Figure 1c shows a greater crystallinity pattern (2θ = 25–28°), decreasing between 60 and 80°. The XRD pattern shows the crystalline phase nature at a diffraction peak of 2θ values of 28.3°, 32.6°, 38.7°, 50.2°, and 59.9°, corresponding

to monoclinic ZrO_2. Generally, ZrO_2 has nanostructures of the monoclinic phase, possesses nanograins, and has a low strain, as shown on the XRD pattern. This finding means the thermal modification process helps to explain the phenomenon of crystallinity along the lower degree, which gives more incredible lactic structure and acidity. $Zr(OH)_2$ in Figure 1b shows less crystallinity than ZrO_2. The XRD pattern shows that the amorphous $Zr(OH)_2$ was less crystalline after calcination than ZrO_2. Thus, this dynamic character of zirconium hydroxide-to-oxide thermal evolution is also in concordance with other authors [23]. The powered content of $Zr(OH)_2$ is high, and the intensity of the peak has a significant peak (2θ = 20–30°), which is the essential nature of the catalyst.

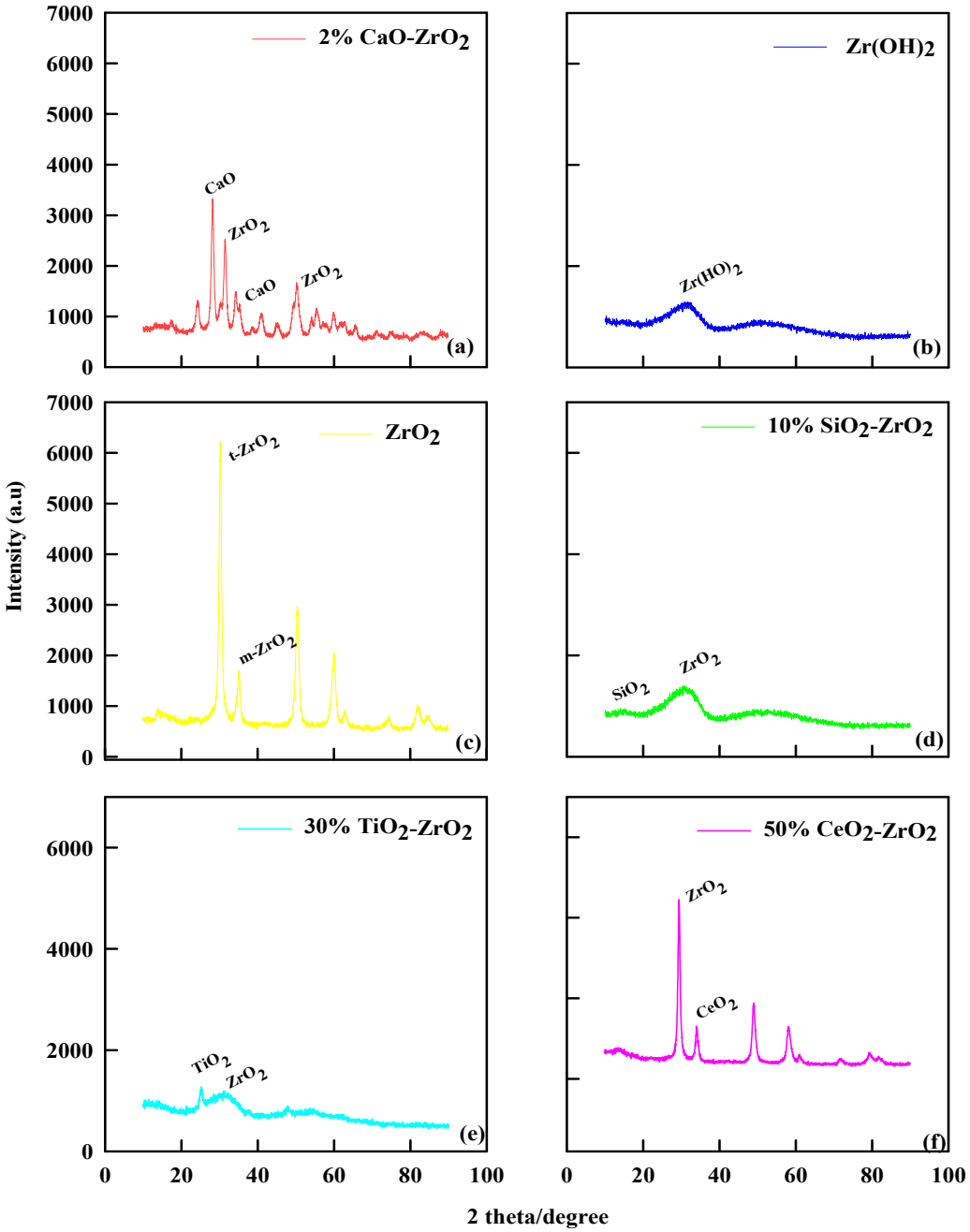

Figure 1. XRD pattern of (**a**) 2% CaO-ZrO_2, (**b**) $Zr(OH)_2$, (**c**) ZrO_2, (**d**) 10% SiO_2-ZrO_2, (**e**) 30% TiO_2-ZrO_2, and (**f**) 50% CeO_2-ZrO_2.

The XRD pattern for 10% SiO_2-ZrO_2 shows a similar trend to $Zr(OH)_2$. The XRD pattern in Figure 1d shows that when the catalyst was calcined at 700 °C, a change in

morphology of the crystal structure of ZrO_2 is typical for the diffraction peak around 10° (2θ), which indicates mesoporous materials. The single diffused peak at 20–30° indicates that 10% SiO_2-ZrO_2 catalyst maintains an amorphous structure at 700 °C calcination. The crystallization of ZrO_2 in the 10% SiO_2-ZrO_2 catalyst was prevented by 10% SiO_2 during the calcining process because Si-O-Zr bonds in 10% SiO_2-ZrO_2 xerogels retard the crystal growth and phase transition [24]. Likewise, for 2% CaO-ZrO_2, as shown in Figure 1a, the XRD pattern shows that the catalyst has either a cubic or a tetragonal phase, which also indicates that CaO was not amorphous nor well dispersed on the surface of the zirconia. The presence of CaO shows a greater degree of crystal pattern and increases the angular lattice point of interaction [25].

For 30% TiO_2-ZrO_2, as shown in Figure 1e, the XRD pattern of pure ZrO_2 was a monoclinic phase, and pure TiO_2 showed an anatase phase, but the mixed oxide of 30% TiO_2-ZrO_2 was found to be X-ray amorphous, as Zou and Lin stated [26]. The XRD pattern of the mixed oxide of 30% TiO_2-ZrO_2 exhibited poor crystallinity with the tetragonal phase of ZrO_2. Generally, under the same catalytic preparation with other commercial catalysts, pure ZrO_2 has a monoclinic phase, but with 30% TiO_2, the component ZrO_2 was stabilized as the tetragonal phase. For 50% CeO_2-ZrO_2, Figure 1f shows that the XRD pattern is highlighted by a peak that appears to be ZrO_2. It was remarkable that the XRD peak positions and lattice parameters of Ce/ZrO_2 were continuously shifted from CeO_2 to ZrO_2 depending on the ratio of Ce/Zr in the precursor solution, as explained by Vegard's law [27]. Thus, from the results, the XRD pattern of 50% CeO_2-ZrO_2 shows that the crystal sizes would be small and homogeneously well dispersed at the XRD detection level. The XRD pattern for 50% CeO_2-ZrO_2 exhibited a mixed profile of cubic CeO_2 and tetragonal ZrO_2 phase.

Generally, the crystallinity of the catalyst was calculated using the XRD data. The equation is as follows:

$$\text{Crystallinity} = \frac{\text{Area of crystalline peaks}}{\text{Area of all peak(crytalline} + \text{Amorphous)}} \times 100 \quad (1)$$

Therefore, the crystallinity of ZrO_2 was 78.3%, showing distinct peaks and hence its crystalline nature. $Zr(OH)_2$ has an amorphous morphology in which its crystallinity was 20.4%; The 2% CaO-ZrO_2 catalyst has a crystallinity of 87.3%, which can also be identified by the many distinct peaks and also the appearance of CaO structures. The 50% CeO_2-ZrO_2 catalyst has a crystallinity of 74.3%. The 30% TiO_2-ZrO_2 catalyst has 30.2% crystallinity, while SiO_2-ZrO_2 has a crystallinity of 28.3%.

2.2. XPS Analytical Profile of the Catalyst

The XPS analyses of catalysts show the mass surface concentration of carbon, oxygen, zirconium, and silicon (C 1s, O 1s, Zr 3d, and Si 2p) (Figure 2). Table 2 lists the percentage of surface oxygen and carbon as about 47.3% and 28.0% for ZrO_2; 53.2% and 23% for 2% CaO-ZrO_2; 53.4% and 19% for 10% SiO_2-ZrO_2; 49.6% and 29% for $Zr(OH)_2$; 54% and 22.8% for 30% TiO_2-ZrO_2 and 51.4% and 24.8% for 50% CeO_2-ZrO_2, respectively. The silicon level is shown as 6.8% in 10% SiO_2-ZrO_2. Meanwhile, 10% SiO_2-ZrO_2 has increased oxygen content compared to all the others. This effect explains the method of catalytic preparation for the commercial catalysts using the treated methods. The carbon content varies from 25% for ZrO_2, which was the highest, to 19% for 10% SiO_2-ZrO_2. Since all the catalysts have some amount of Zr, this effect influences ethanol conversion in various degrees, from 25% for ZrO_2 to the lowest 20.9% for 10% SiO_2-ZrO_2.

Comparing the spectra lines shows the band energies for Zr 3d and Si 2p. Different binding energies are associated with each species, between 140 to 200 eV for Zr 3d, 105 to 100 eV for Si 2p, Ti 2p has a binding energy of 459 eV, and Ce 3d has a binding energy of 884.5 eV. The decrease in the nature of the peak level for Si 2p shows the desilication of the silicon group in the catalytic preparation methods. It indicated the performance of

the catalyst during the reaction. The peak, shifting from the maximum binding energies, indicated oxidized silicon elements' general direct proportional ratio.

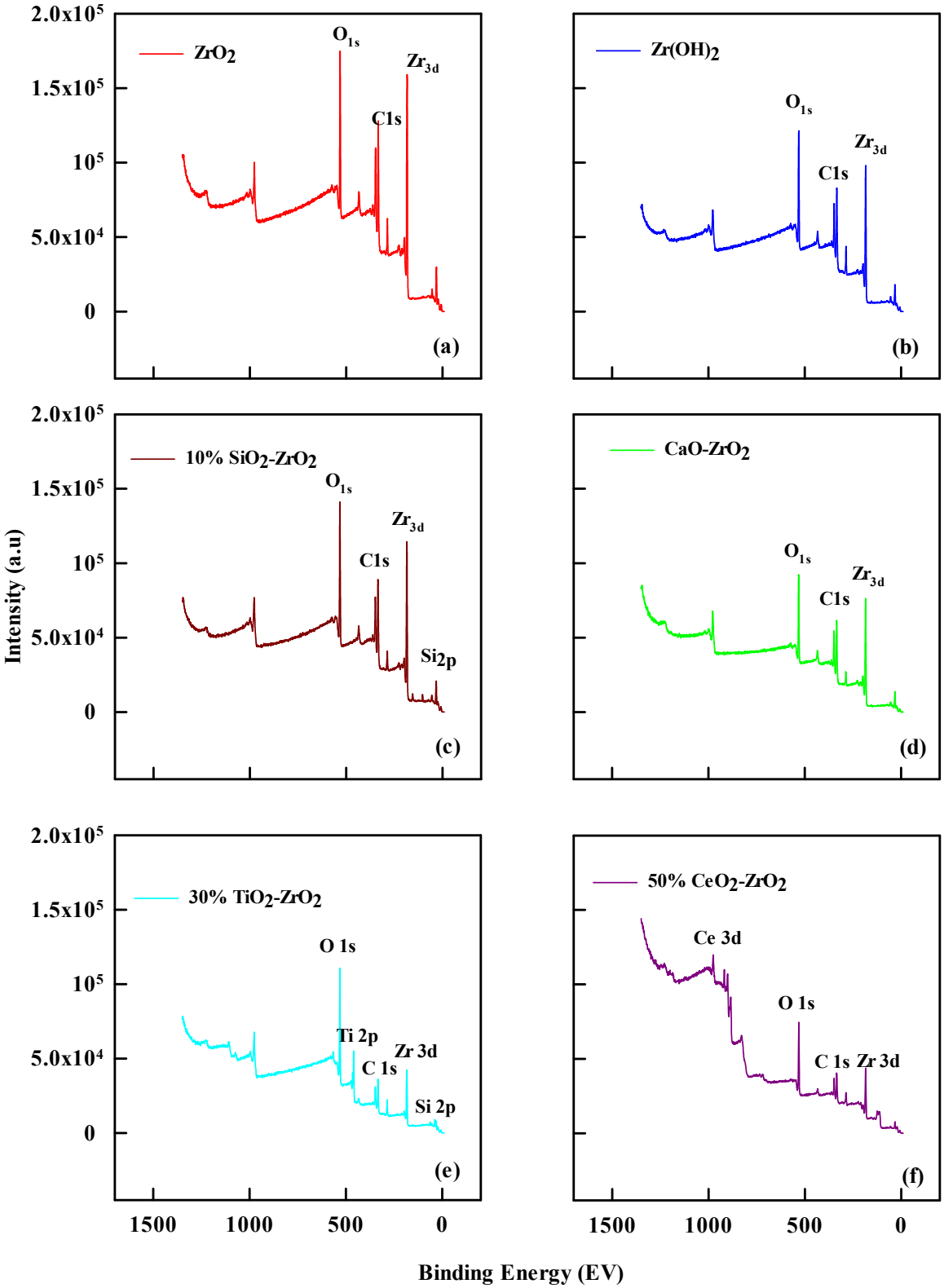

Figure 2. XPS profile for (**a**) ZrO_2, (**b**) 10% SiO_2-ZrO_2, (**c**) $Zr(OH)_2$ (**d**) 2% CaO-ZrO_2 (**e**) 30% TiO_2-ZrO_2, and (**f**) 50% CeO_2-ZrO_2.

Table 2. Weight percentage (%) of the elements by XPS analysis.

Catalyst	O 1s (%)	C 1s (%)	Zr 3d (%)	Si 2p (%)	Ca 2p (%)	Ti 2p (%)	Ce 3d (%)
ZrO_2	47.3	27.9	24.9	-			
2% CaO-ZrO_2	50.3	23.0	23.8	-	2.9		
10% SiO_2-ZrO_2	53.4	19.0	20.9	6.8			
$Zr(OH)_2$	49.6	29.0	21.4	-			
30% TiO_2-ZrO_2	54	22.8	10.7	2.3		10.3	
50% CeO_2-ZrO_2	51.4	24.8	13.4				10.4

2.3. BET Profiles of the Catalyst

Figure 3 shows the relative pore-diameter distribution of the catalyst before and after the reaction. The characterization of the pore volume was investigated by N_2 adsorption-desorption methods. Tables 3 and 4 list the surface area and pore volume of the catalyst before and after the reaction. For the ZrO_2 sample, the pore volume (V_{meso}) of 0.0012 cm^3/g increased to 0.0014 cm^3/g after the reaction. The surface area of ZrO_2 (S_{BET}) was 98 m^2/g before the reaction. It decreased to 78 m^2/g after the reaction. $Zr(OH)_2$ has a pore area of 50 m^2/g and micro-pore volume of 0.004 cm^3/g, which went down to 32 m^2/g and 0.002 cm^3/g after the reaction. The 10% SiO_2-ZrO_2 catalyst has a surface area of 90 m^2/g and micro-pore volume of 0.0172 cm^3/g, decreasing to 88 m^2/g and 0.142 cm^3/g after the reaction. The 2% CaO_2-ZrO_2 catalyst has a surface area of 195 m^2/g and micro-pore volume of 0.006 cm^3/g, down to 100 m^2/g and 0.004 cm^3/g. For 30% TiO_2-ZrO_2, a surface area of 293 m^2/g and micro-pore volume of 0.0093 cm^3/g decreased to 212 m^2/g and 0.0087 cm^3/g after the reaction.

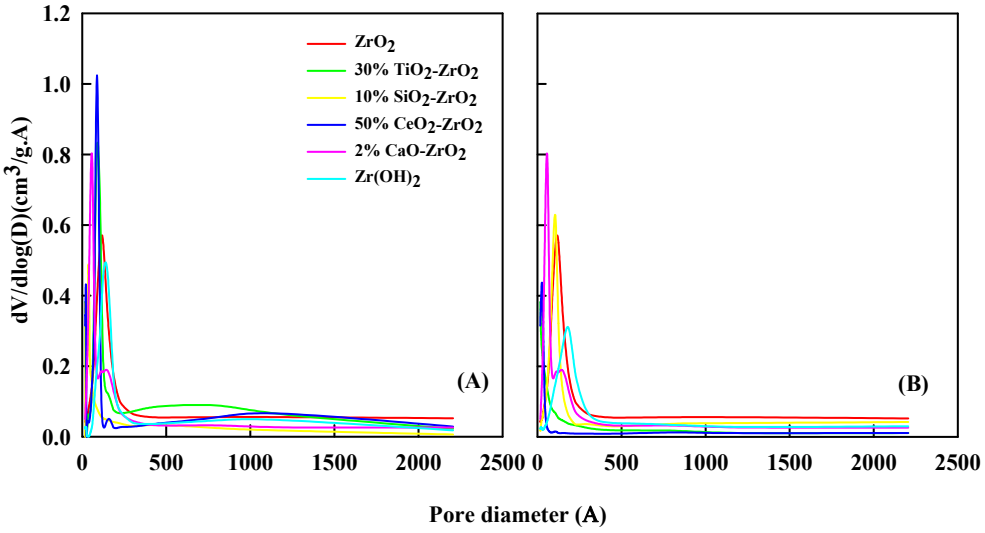

Figure 3. Pore-size distribution of treated catalyst (**A**) before reaction and (**B**) after reaction.

Table 3. Catalyst particle size and BET surface area before reaction.

Catalyst	Surface Area (m^2/g)			Pore Volume (cm^3/g)	
	S_{BET} [a]	S_{micro} [b]	S_{ext} [b]	V_{micro} [b]	V_{meso} [c]
ZrO_2	98	-	116	-	0.0012
$Zr(OH)_2$	50	5.5	45	0.0004	0.0002
2% CaO-ZrO_2	195	3.4	191	0.0006	0.0004
10% SiO_2-ZrO_2	90	7.4	83	0.0172	0.0013
30% TiO_2-ZrO_2	293	43	250	0.0093	0.0063
50% CeO_2-ZrO_2	205	-	218	-	0.0044

[a] BET method, [b] t-Plot method, [c] BJH method (adsorption branch).

Table 4. Catalyst particle size and BET surface area after the reaction.

Catalyst	Surface Area (m^2/g)			Pore Volume (cm^3/g)	
	S_{BET} [a]	S_{micro} [b]	S_{ext} [b]	V_{micro} [b]	V_{meso} [c]
ZrO_2	78	-	89	-	0.0014
$Zr(OH)_2$	32	3.2	16	0.0002	0.0005
2% CaO-ZrO_2	100	1.6	78	0.0004	0.0008
10% SiO_2-ZrO_2	88	6.8	100	0.0142	0.0015
30% TiO_2-ZrO_2	212	12.8	145	0.0087	0.0093
50% CeO_2-ZrO_2	178	-	164	-	0.0056

[a] BET method, [b] t-Plot method, [c] BJH method (adsorption branch).

The higher loss of micro-pore area in catalysts suggests that the coke precursors or coke produced during the reaction procedure tend to deposit in the newly created micro-pores. The deposition of coke could be due to the formation of ash. If the catalyst is exposed to a high temperature for a long time, the ash or coke deposition can affect the reactivity, decreasing the pore size or altering it, as suggested in previous literature [28,29]. Consequently, the newly created micro-pores may quarter the part of coke deposition, sinking the materialization of coke deposition in its inherent micro-pores to some extent. The coke deposition causes the decrease of S_{micro} and V_{micro}. The strait obstruction by coke deposition over the prepared catalyst limits the access of reactants/intermediates to the core active sites on the catalyst. The surface area and pore volume size will distress the catalyst for ethanol to 1,3-butadiene reaction. The coke deposition effect will be amplified when the surface area and pore volume are small. When the coke effect is strong, the catalyst activity will be decreased. Because the coke effect will block the surface area and pore volume, the catalyst will be less active.

2.4. Measurement of Catalyst Deposition and Regeneration Using TGA

For the coke decomposition of the catalyst after reaction, TGA analysis was performed on ZrO_2, $Zr(OH)_2$, CaO-ZrO_2, and 10% SiO_2-ZrO_2. As shown in Figure 4, the total weight loss follows a trend up to 800 °C. The weight loss of the catalysts is given as follows: ZrO_2 has a weight loss of 4 wt%; $Zr(OH)_2$ has a weight loss of 19 wt%; 2% CaO-ZrO_2 has a weight loss of 2 wt%, and 10% SiO_2-ZrO_2 has a weight loss of 9 wt%.

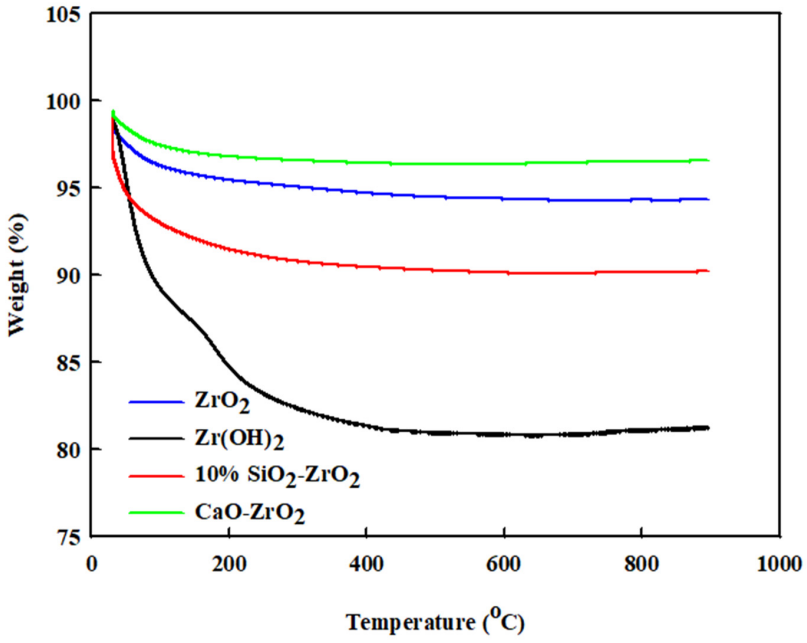

Figure 4. TGA-profile analysis for ZrO_2, $Zr(OH)_2$, CaO-ZrO_2 and 10% SiO_2-ZrO_2.

Generally, if the catalyst loses weight at a lower temperature (i.e., below 170 °C), it is normally associated with the effect of water absorption, since the catalysts are porous in many aspects. The weight loss is due to the burning of the catalyst, which could lead to the accumulation of coke at 250–800 °C in the reactor. $Zr(OH)_2$ shows a more significant amount of coke decomposition than all the others. The 2% CaO-ZrO_2 catalyst has more thermal stability compared to other catalytic systems. Hence, it has low coke formation. The TGA profile also shows some regenerative nature in all the catalysts (ZrO_2, $Zr(OH)_2$, 2% CaO-ZrO_2, and 10% SiO_2-ZrO_2) because the weight loss remains mostly constant for each of them at 200 °C. The TGA profiles also help to show that the ZrO_2-containing catalyst has a good regeneration characteristic and thermal stability. A TGA sample for each catalyst was taken, and some present a similar pattern: 30% TiO_2-ZrO_2 has a similar curve to 2% CaO-ZrO_2, and 50% CeO-ZrO_2 has a similar curve to ZrO_2. This finding demonstrates that they have similar thermo-stability but different relativities, see Figure S2 in Supplementary Materials.

2.5. Effect of Weight Hourly Space Velocity (WHSV)

Ethanol dehydration using catalysts dramatically affects the yield of 1,3-butadiene at different WHSV. Space velocity is an essential factor in catalytic activity and explains the concentration profiles [30]. The production rate of 1,3-butadiene is directly proportional to ethanol's WHSV [31]. Mass transfer increases are effective, resulting from increased space velocity and gas velocity [9].

2.5.1. Effect of Catalyst at WHSV = 2.5 h^{-1}

Figure 5 and Table 5 show the performance of different pretreated commercial catalysts at different temperatures at WHSV = 2.5 h^{-1}. The ethanol dehydration is incomplete at lower temperatures; thus, ethanol conversion was low. The ethanol conversion was 40% at 250 °C for ZrO_2, while the ethanol conversion increased to 60% at 400 °C. The same trend can be observed for $Zr(OH)_2$, which shows 10% ethanol conversion at 250 °C and 22% at 350 °C, but at 400 °C, the ethanol conversion drops to 8%. This finding could be explained by the coke decomposition of the $Zr(OH)_2$. For 10% SiO_2-ZrO_2, ethanol conversion was 50% at 250 °C, while ethanol conversions were 90% and 90% at 300 and 350 °C, respectively. CaO-ZrO_2 shows an ethanol conversion of 40% at 250 °C and 79% at 300 °C, respectively.

The product yields follow a different trajectory at WHSV of 2.5 h^{-1}, ZrO_2 catalytic performance shows a 25% yield of 1,3-butadiene at 250 °C and 30% yield at 300 and 350 °C, respectively, and at 400 °C, it drops to 20%. Moreover, ZrO_2 gave better acetaldehyde 20% yield at 300 and 350 °C, although it decreased to 14% when the temperature was 400 °C. The ethylene yield was 6% at 250 °C and 10% at 350 °C. This result was due to the structural morphology of the catalyst and its crystalline nature, which will effectively favor more of an acidic reaction, and this effect will resist any new active sites to be developed on the catalyst unless further modification takes over. For $Zr(OH)_2$, 1,3-butadiene yield is 18% at 250 °C, and shows a little increase at 350 °C (20%) and at 400 °C (22%). The acetaldehyde yield was 10% at 250 °C, and it eventually increased to 14% at 350 °C and 400 °C, respectively. The ethylene yield was 24% at 350 °C.

The 2% CaO-ZrO_2 catalyst favors an ethanol conversion of 40% at 250 °C and 80% at 300 and 350 °C, respectively, which shows a steady-state mechanism. Ethanol conversion decreases to 60% at 400 °C. It generates a 1,3-butadiene yield of 30% at 350 °C and an acetaldehyde yield of 15% at 300 and 350 °C. It gives an ethylene yield of 30% from 250 to 350 °C. This result is in concordance with [30] for ethylene production. The 10% SiO_2-ZrO_2 catalyst gives an ethanol conversion of 50%, 90%, 90% and 87% at 250, 300, 350 and 400 °C, respectively. The highest 1,3-butadiene yield was 80% at 350 and 400 °C. The combination of SiO_2 and ZrO_2 tends to favor more ethylene production (9.8% at 300 °C) than acetaldehyde.

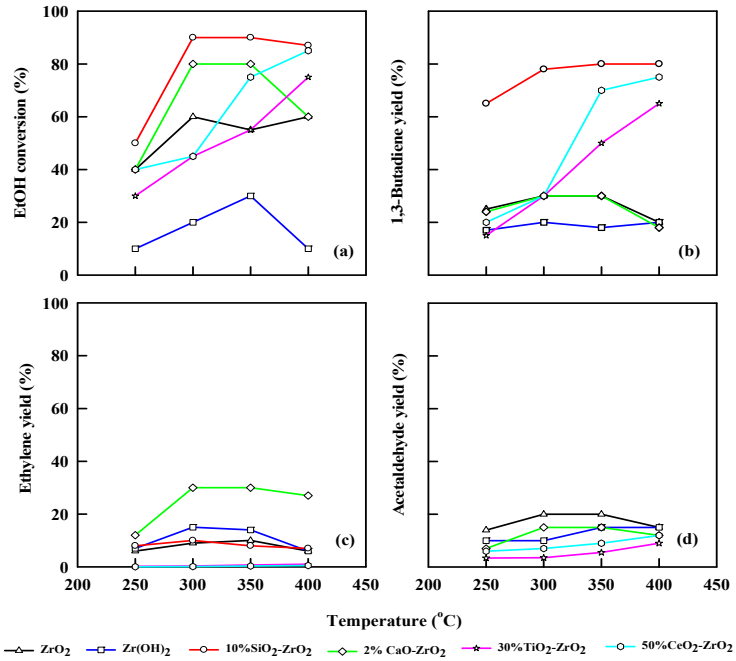

Figure 5. Plot of ethanol conversion (**a**), yields of 1,3-butadiene (**b**), ethylene (**c**), and acetaldehyde (**d**) vs. reaction temperature for different pretreated commercial catalysts. WHSV: 2.5 h^{-1}, catalyst: 0.4 g, N_2: 30 mL/min.

Table 5. STY of 1,3-butadiene using different temperatures and pretreated catalysts.

		WHSV (h^{-1})	
Catalyst	**T (°C)**	**1.25**	**2.5**
ZrO_2	250	256	456
	300	328	528
	350	343	503
	400	87.6	97.6
$Zr(OH)_2$	250	79.7	99.7
	300	189	199
	350	284	204
	400	278	308
2% CaO-ZrO_2	250	348	231
	300	457	346
	350	468	408
	400	85.6	89.3
10% SiO_2-ZrO_2	250	549	449
	300	557	589
	350	566	578
	400	580	558
30% TiO_2-ZrO_2	250	87.2	98.7
	300	212	412
	350	329	423
	400	399	489
50% CeO_2-ZrO_2	250	99.7	249
	300	254	348
	350	444	459
	400	522	579

Catalyst: 0.4 g, T (Temperature), X (Conversion), Y (Yield), STY (Space time yield) (gKg^{-1} h^{-1}).

For ZrO_2, the 1,3-butadiene yield was 23% at 250 °C, and the space-time yield (STY) was 456 gKg^{-1} h^{-1}. The STY decreased when the temperature was 400 °C (97.6 gKg^{-1} h^{-1}). $Zr(OH)_2$ has a STY of 308 gKg^{-1} h^{-1} when the temperature was increased from 350 to 400 °C, and the 1,3-butadiene yield attained was 20%. CaO-ZrO_2 shows a steady yield

of 1,3-butadiene at 250 to 350 °C with a 30% yield, and the STY increases from 346 to 408 gKg^{-1} h^{-1}. The 10% SiO_2-ZrO_2 catalyst has 80% 1,3-butadiene yield, and the STY increased from 449 gKg^{-1} h^{-1} at 250 °C to 578 gKg^{-1} h^{-1} at 350 °C. At 400 °C, 30% TiO_2 combined with ZrO_2 realized an ethanol conversion of 79% with 65% 1,3-butadiene yield. The 1,3-butadiene yield increases with an increase in temperature from 250–400 °C, and the STY increases from 98.7 to 489 gKg^{-1} h^{-1} as temperature increases from 250 to 400 °C. The same trend was observed for 50% CeO_2-ZrO_2 with 90% ethanol conversion at 400 °C and 2.5 h^{-1} WHSV. The 1,3-butadiene yield increases with an increase in temperature. The highest yield of 1,3-butadiene for CeO_2-ZrO_2 was 79% at 400 °C. An increase in temperature also increases STY for CeO_2-ZrO_2 (249–579 gKg^{-1} h^{-1}), as shown in Table 5.

2.5.2. Effect of Catalyst at WHSV = 1.25 h^{-1}

Figure 6 and Table 5 show the different modified commercial catalysts' performances at different temperatures and WHSV of 1.25 h^{-1}. For ZrO_2, the modified catalyst, in this instance, converted ethanol to a maximum of 60% at 350 °C. The 1,3-butadiene yield was 30% at 350 °C, acetaldehyde yield was 20% at 350 °C, and ethylene yield was 9.7% at 350 °C. $Zr(OH)_2$ generates an ethanol conversion of 39% at 350 °C, and 1,3-butadiene yield of 20% at 300 °C. The ethylene yield was 10%, while acetaldehyde was 14% at 350 °C. The 2% CaO-ZrO_2 catalyst produces an ethanol conversion of 80% at 350 °C and a 1,3-butadiene yield of 30% at 350 °C. The acetaldehyde yield was 14% at 300 °C. Surprisingly, it yields more ethylene (30%) at 350 °C than acetaldehyde. This effect was due to the presence of CaO, which allows the catalyst to behave with a more amphiprotic nature. The 10% SiO_2-ZrO_2 catalyst gives an ethanol conversion of 90% at 300 °C and 80% yield of 1,3-butadiene at 300 to 400 °C, respectively. It also gives an ethylene yield of 8.9% at 350 °C. Acetaldehyde yield was less noticeable during this catalytic reaction.

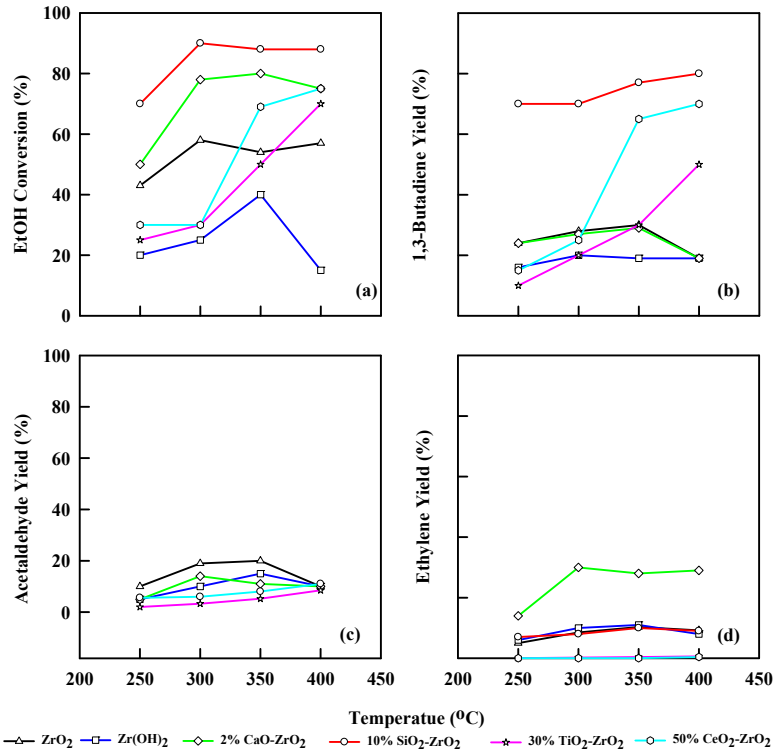

Figure 6. Plot of ethanol conversion (**a**), yields of 1,3-butadiene (**b**), acetaldehyde (**c**), and ethylene (**d**) vs. reaction temperature for different modified commercial catalysts. WHSV: 1.25 h^{-1}, catalyst: 0.4 g, N_2: 30 mL/min.

When WHSV is 1.25 h^{-1}, ZrO_2 has a 1,3-butadiene yield of 21% and STY of 256 $gkg^{-1}h^{-1}$ at 250 °C. The yield of 1,3-butadiene increases by 28% at 350 °C and a STY of 343 $gkg^{-1}h^{-1}$.

When the temperature increases to 400 °C, the STY decreases to 87.6 $gkg^{-1}h^{-1}$, and the 1,3-butadiene yield drops to 15%. Using $Zr(OH)_2$ generated 20.8% butadiene yield at 400 °C and 278 $gkg^{-1}h^{-1}$ STY, compared to ZrO_2, which yielded less. CaO-ZrO_2 has a 1,3-butadiene yield of 39% at a STY of 468 $gkg^{-1}h^{-1}$ at 350 °C, but at 400 °C, the STY is decreased to 85.6 $gkg^{-1}h^{-1}$. The 10% SiO_2-ZrO_2 catalyst has a good 1,3-butadiene yield of 70% at 350 °C and STY of 580 $gkg^{-1}h^{-1}$.

The ethanol conversion at WHSV = 1.25 h^{-1} for TiO_2-ZrO_2 shows a similar trend to WHSV of 2.5 h^{-1}, but there was a decrease in the total ethanol conversion, which was 65% at 400 °C compared to 2.5 h^{-1}, which was 79% at 400 °C. However, the general increase in ethanol conversion was realized as the temperature increased from 250–400 °C. The 1,3-butadiene yield was 50% at 400 °C, the highest for TiO_2 catalyst at 1.25 h^{-1}. Acetaldehyde and ethylene yields were 8% and 0.2%, respectively, at 400 °C. The STY was increased from 87.2 $gkg^{-1}h^{-1}$ at 250 °C to 399 $gkg^{-1}h^{-1}$ at 400 °C for TiO_2-ZrO_2. CeO_2-ZrO_2 has an ethanol conversion of 79% and 1,3-butadiene yield of 65% at 400 °C. The acetaldehyde and ethylene yields were 12% and 0.3% at 350 °C. Also, an increase in STY was observed from 250 °C–400 °C (99.7–52 $gkg^{-1}h^{-1}$) (Table 5) for CeO_2-ZrO_2.

2.5.3. Effect of Catalyst at WHSV = 6.0 h^{-1}

Figure 7 illustrates the performance of different modified catalysts for different temperatures at WHSV of 6.0 h^{-1}. Likewise, ZrO_2 produces an ethanol conversion of 59% at 350 °C and a 1,3-butadiene yield of 30% at the same temperature. The acetaldehyde yield was 30% at 300 °C, while the ethylene yield was 5% at 350 °C. $Zr(OH)_2$ shows an ethanol conversion of 43% at 350 °C and a 1,3-butadiene yield of 19.2%. Acetaldehyde and ethylene yields were 14% and 5%, respectively, at 350°C. CaO-ZrO_2 has a combination effect, generating an ethanol conversion of 80% at 350 °C, but ethanol conversion decreases to 67% at 400 °C. The 1,3-butadiene yield increases steadily from 20% at 250 °C up to 30% at 350 °C and, eventually, it decreases to 18% at 400 °C. The 10% SiO_2-ZrO_2 catalyst shows a greater ethanol conversion of 90% and 1,3-butadiene yield of 80% at 350 °C. Ethylene yield was 9.5% at 300 °C.

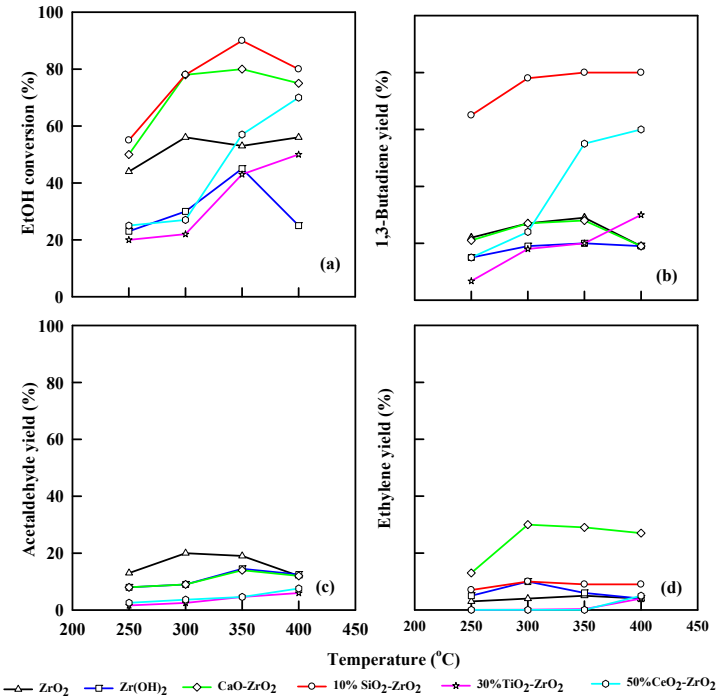

Figure 7. Plot of ethanol conversion (**a**), yields of 1,3-butadiene (**b**), acetaldehyde (**c**), and ethylene (**d**) vs. reaction temperature for different modified commercial catalysts. WHSV: 6.0 h^{-1}, catalyst: 0.4 g, N_2: 30 mL/min.

TiO_2-ZrO_2 has an ethanol conversion of 43% and 25% 1,3-butadiene yield. The ethanol conversion was stable as the temperature was increased from 250 to 300 °C, but it increased from 20% to 43% as the temperature was increased from 350 to 400 °C. The increase in temperature also leads to an increase in 1,3-butadiene yield. Acetaldehyde yield was 5.5%, while ethylene yield was 0.3% at 400 °C. CeO_2-ZrO_2 converted ethanol to 70% at WHSV of 6.0 h^{-1} and 400 °C, while it yielded 60% 1,3-butadiene. Acetaldehyde and ethylene yields were 7.7% and 0.5%, respectively.

2.5.4. Effect of WHSV of Ethanol at 0.75 h^{-1}

Figure 8 demonstrates the effect of 0.75 h^{-1} WHSV of ethanol during the catalytic dehydration using different modified commercial catalysts. ZrO_2 catalyst gave an ethanol conversion of 50% to 55% at 350 °C and 400 °C, respectively, and 1,3-butadiene yield of 22% at 350 °C. Alternatively, the yield of acetaldehyde was 19% at 300 °C, and ethylene yield was 5% at 400 °C. $Zr(OH)_2$ realized an ethanol conversion of 50% at 300 °C and a 1,3-butadiene yield of 20% at 400 °C. At 350 °C, WHSV of 0.75 h^{-1}, ZrO_2 catalyst yielded 8% and 6% of acetaldehyde and ethylene, respectively, while CaO-ZrO_2 generated 69% ethanol conversion with 23% 1,3-butadiene yield. 10% SiO_2-ZrO_2 catalyst shows an excellent ethanol conversion of 90% at 350 °C and 80% 1,3-butadiene yield.

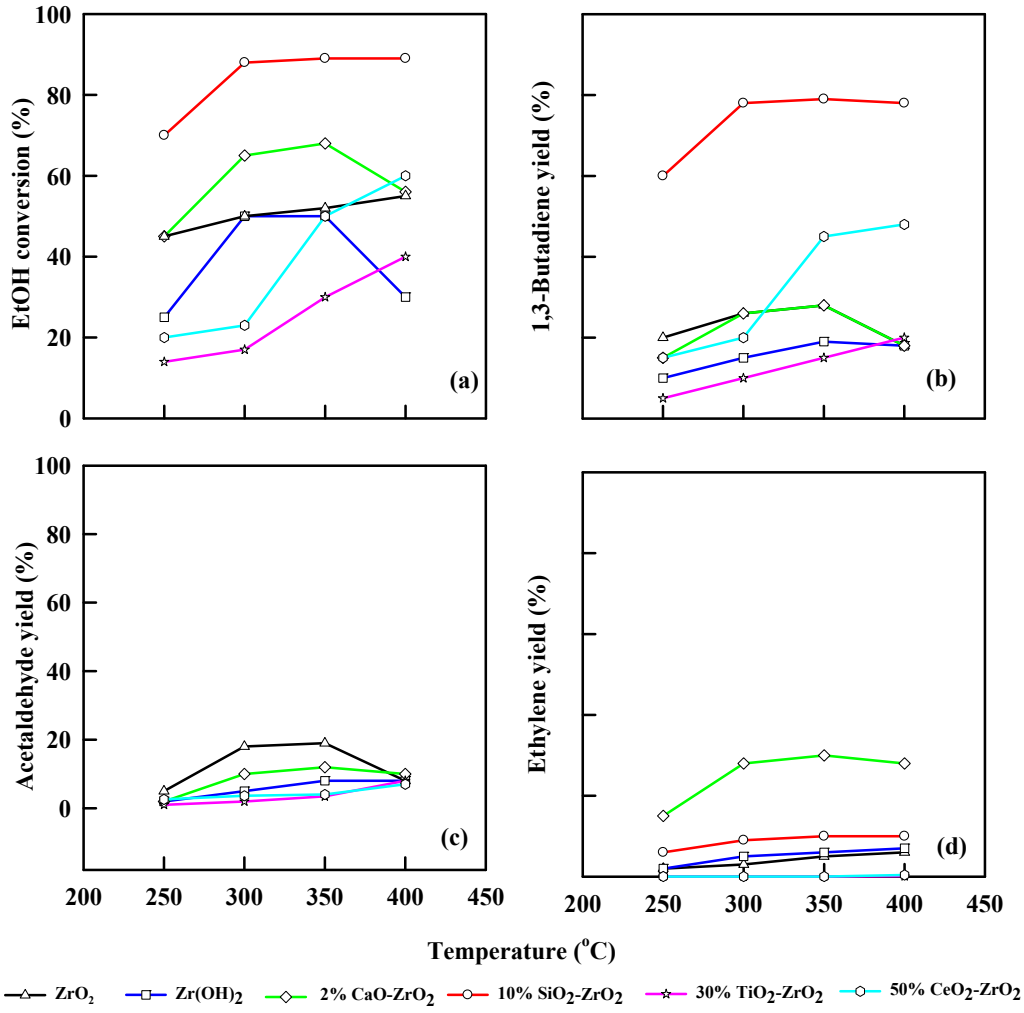

Figure 8. Plot of ethanol conversion (**a**), yields of 1,3-butadiene (**b**), acetaldehyde (**c**), and ethylene (**d**) vs. reaction temperature for different modified commercial catalysts. WHSV: 0.75 h^{-1}, catalyst: 0.4 g, N_2: 30 mL/min.

At 0.75 h^{-1} WHSV, 30% TiO_2-ZrO_2 yielded 40% ethanol and realized a 25% 1,3-butadiene yield, while acetaldehyde and ethylene yield were 6% and 4%, respectively, at 400 °C. CeO_2-ZrO_2 shows an ethanol conversion of 67% and 1,3-butadiene yield of 60% at 400 °C and 0.75 h^{-1} WHSV. Acetaldehyde yield increases linearly from 1.0% to 3.0% as temperature increases from 250–350 °C, while ethylene yield remains constant as temperature increases from 250–400 °C. The TiO_2/CeO_2-ZrO_2 catalytic system shows an increase in STY as temperature increases.

2.6. Comparing the Effect of Treated and Untreated Commercial Catalysts

The treatment of ZrO_2 parent catalyst with its substituent (SiO_2, TiO_2, CaO, or CeO_2) was conducted for ethanol dehydration to 1,3-butadiene, as shown in Table 6. The process used to treat the Zr-catalyst and its combination was conducted using 0.2 M NaOH, NH_4NO_3, and 0.5 M oxalic acid solution, as explained in the catalyst preparation methods. These reagents provide either desilication, basic and acidic sites, Lewis acidic and basic sites that are needed for the catalytic ethanol to 1,3-butadiene production [11,32,33]. By comparing the output of ethanol conversion, the treated-commercial catalyst yielded higher ethanol conversion than the un-treated commercial catalyst.

Table 6. Performance summary of treated and untreated commercial catalyst at 350 °C.

	[a] Treated	[b] Untreated	[c] Treated	[d] Untreated
Catalyst	**X_{EtOH} (%)**	**X_{EtOH} (%)**	**$Y_{1,3\text{-butadiene}}$ (%)**	**$Y_{1,3\text{-butadiene}}$ (%)**
ZrO_2	60	34.5	30	10.6
$Zr(OH)_2$	50	30.4	20	10
2% CaO-ZrO_2	79.8	37.3	30	15.7
10% SiO_2-ZrO_2	88.8	40.6	75.9	20.3
30% TiO_2-ZrO_2	70.7	47	55	19.5
50% CeO_2-ZrO_2	74.5	47	65.3	16.8

[a] X_{EtOH}: ethanol conversion for treated catalyst, [b] X_{EtOH}: ethanol conversion for untreated catalyst, [c] $Y_{1,3\text{-butadiene}}$: 1,3-butadiene yield for treated catalyst, [d] $Y_{1,3\text{-butadiene}}$: 1,3-butadiene yield for untreated catalyst, WHSV = 0.75 h^{-1}.

2.7. Effect of Time on Stream on Ethanol Dehydration

Figure 9 show the stability of the following catalysts, ZrO_2, $Zr(OH)_2$, 2% CaO-ZrO_2, 30% TiO_2-ZrO_2, 50% CeO_2-ZrO_2 and 10% SiO_2-ZrO_2. The conversion of ethanol and selectivity of 1,3-butadiene decreases with time. The parent catalyst ZrO_2 as an acidic catalyst and $Zr(OH)_2$ as the basic catalyst show a lower ethanol conversion than 2% CaO-ZrO_2 and 10% SiO_2-ZrO_2. The results highlight that ZrO_2 has a selectivity of 57% at 10 h, and $Zr(OH)_2$ has a selectivity of 40% at 10 h time on streams. The introduction of CaO into the ZrO_2 catalytic system promotes the formation of extra dehydrogenation sites, making the acetaldehyde condensation site, hence the rate-limiting step. The presence of SiO_2 to ZrO_2 aids in increasing the yield of 1,3-butadiene. However, a limited amount of SiO_2 (10%) is needed during this reaction because it will promote the diffusion of the metals on the surface of the catalyst, and assists the formation of the active site for dehydration of ethanol and crotyl alcohol reaction to 1,3-butadiene; thus, the selectivity of 1,3-butadiene was 90%.

TiO_2, in combination with ZrO_2, as a catalytic system, gains more stability, and the selectivity of 1,3-butadiene was 87%. The presence of CeO_2 has a significant effect because CeO_2 has both Brønsted basic and Lewis basic sites, which aid in the creation of new active sites during the reaction and poisons some acidic sites at high temperatures 1,3-butadiene production to be realized. The 10% SiO_2-ZrO_2 catalytic system shows better stability than other commercial catalysts.

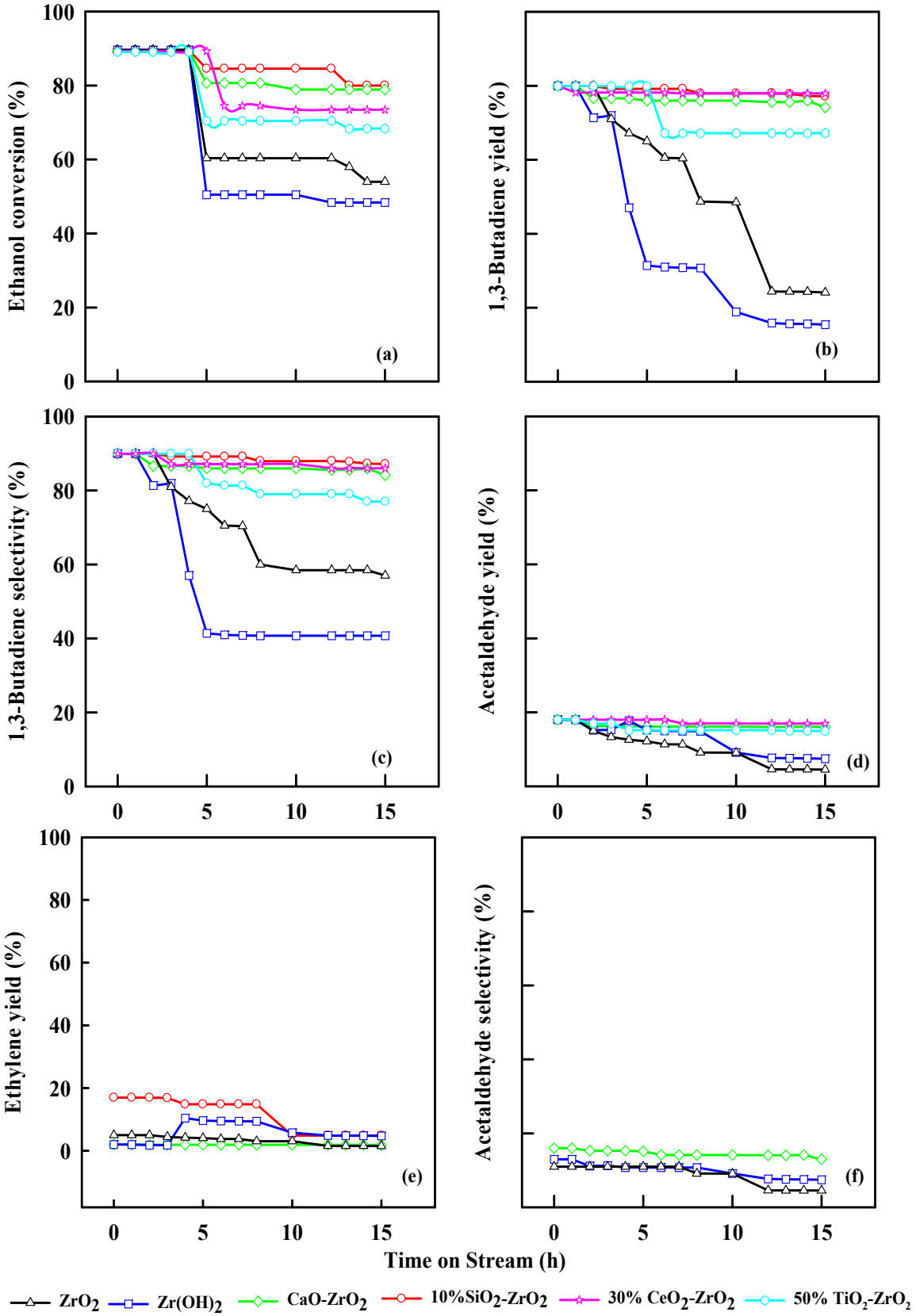

Figure 9. Conversion of ethanol (**a**), yield of 1,3-butadiene (**b**), selectivity of 1,3-butadiene (**c**), yields of acetaldehyde (**d**), yield of ethylene (**e**), and selectivity of acetaldehyde (**f**) with time on streams. WHSV: 2.5 h^{-1}, 0.4 g of catalyst, N_2 = 30 mL/min, Temp: 350 °C.

3. Materials and Methods

3.1. Materials

The catalysts of ZrO_2, $Zr(OH)_2$, CaO-ZrO_2, and 10% SiO_2-ZrO_2 were purchased from Daiichi Kigenso Kagaku Kogyo (Tokyo, Japan), ethanol (98%) from Echo Chemical (Miaoli, Taiwan), acetone and sodium hydroxide (NaOH) from Sigma Aldrich (St Louis, MO, USA), hydrochloric acid and ammonium phosphate from Sigma (Utah's Salt Lake, UT, USA), and 1,3-butadiene (10% in nitrogen) and ethylene (10% in nitrogen) from Ming Yang (Taoyuan, Taiwan). The commercial catalysts were treated with oxalic acid in combination with NaOH in a mole ratio of 2:1. The dried samples were then used for all the preparation of the catalysts.

3.1.1. Preparation of ZrO_2 Catalyst

Treated-ZrO_2 commercial catalyst (5 g) was mixed with 50 mL distilled water. The solution was filtered, and the residue was dried for 3 h in an oven. Later the residue was dissolved into dilute HCl (0.05 mol), filtered, and dried for 4 h. Finally, the mixture was calcined under air at 500 °C for 12 h.

3.1.2. Preparation of $Zr(OH)_2$ Catalyst

Treated-$Zr(OH)_2$ commercial catalyst (6 g) was added to 40 mL $ZrCl_4$ in a beaker and rested for 1 h, and then, 0.2 M NaOH was added and mixed vigorously for 30 min. The mixture was filtered, and the residue dried in an oven for 24 h at 60 °C. The solid white power $Zr(OH)_2$ was calcined at 550 °C for 24 h.

3.1.3. Preparation of 10% SiO_2-ZrO_2 Catalyst

Treated-10% SiO_2-ZrO_2 was pretreated using a 0.4 M of acidic oxalic solution. The commercial sample (2.0 g) was added to the NaOH aqueous solution (2.0 M, 100 mL). The solution was heated to 100 °C for 4 h. Then, the sample was dried at 150 °C for 8 h in an oven. The residue was later calcined at 500 °C for 24 h.

3.1.4. Preparation of 2% CaO-ZrO_2 Catalyst

Treated-CaO-ZrO_2 (7 g) was mixed with 0.5 M acetone in a 100 mL volumetric flask. The sample was later dried and gently added to 0.1 M of NaOH solution, and the solution rested for 3 h. Then, the solution was filtered and dried for 24 h in an oven. Finally, the dried sample was calcined at 450 °C for 24 h.

3.1.5. Preparation of 30% TiO_2-ZrO_2 Catalyst

Treated-30% TiO_2-ZrO_2 (4 g) was mixed with 100 mL distilled water and stirred for 1 h. The mixture was filtered and this was followed by the addition of 2.0 M NaOH in 100 mL aqueous solution, and the mixture was left to stand for 12 h. The solution was filtered and dried at 80 °C for 24 h. The sample was later calcined at 500 °C for 14 h.

3.1.6. Preparation of 50% CeO_2-ZrO_2 Catalyst

Treated-50% CeO_2-ZrO_2 consists of tetragonal ZrO_2, which in combination with CeO_2 produces CeO_2-ZrO_2. The commercial catalyst (5 g) was added into a $ZrO(NO_3)_2$ solution (100 mL, 0.5 M). The solution was stirred at 25 °C for 1 h and allowed to settle for 24 h. Later the precipitate was filtered and washed with deionized water and dried at 100 °C for 48 h. The sample was calcined at 500 °C for 5 h in air. Thus, the process was conducted to form CeO_2 with monoclinic ZrO_2 as support during the catalytic reaction. CeO_2 was impregnated into ZrO_2 to obtain precursors.

3.2. Dehydration of the Ethanol Using Fixed Bed Reactor

Ethanol dehydration to 1,3-butadiene is mainly an endothermic chemical reaction process involving more heat energy and higher temperatures, as shown in Figure 10. The reaction temperature is vital in this process because it gives the product selectivity. In

this case, 1,3-butadiene is the target product while other products are expected, such as ethylene and acetaldehyde, mostly termed as byproducts. The main product expected for ethanol dehydration at lower temperatures was acetaldehyde or ethylene. At higher temperatures, such as 350 °C the yield of 1,3-butadiene was realized, and also the method of reactor design determines the selection of the main product. Following the specifics, dehydration of ethanol was conducted with a fixed-bed reactor.

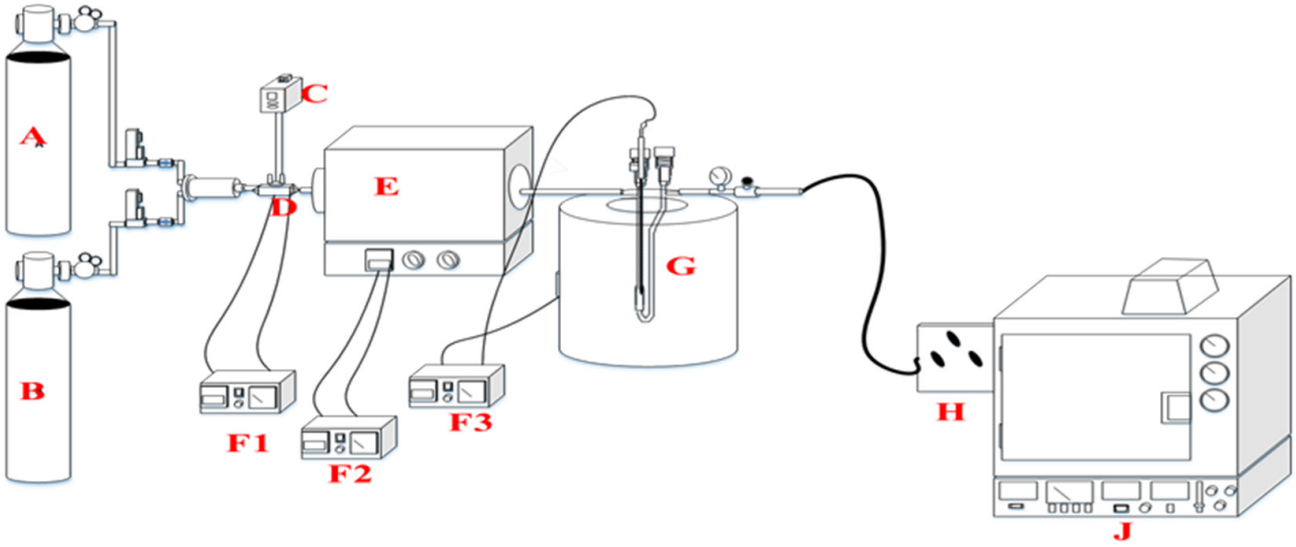

Figure 10. Schematic flow of the reactor design: A: N_2, B: H_2, C: pump, D: evaporator, E: evaporator, F1–F3: temperature controller, G: fixed-bed reactor in the furnace, H: gas sample, J: gas chromatography.

The determination of ethanol was determined with the aid of a gas chromatography−flame ionization detector (GC−FID; GC 14B, Shimadzu, Kyoto, Japan) equipped with a column of Porapak-Q-141023J (length, 3 m; diameter: 2 mm; and film, 1 µm; Quadrex, Bethany, CT, USA) under nitrogen carrier gas (30 mL/min), with N_2 as the gas carrier. The oven conditions were 60–150 °C in temperature with a 10 °C/min ramp rate. The sample was analyzed using a continuous system directly connected to the gas chromatogram. The data were collected depending on the time interval needed.

3.3. Analytical Method for Determination of Ethanol Conversion and 1,3-Butadiene Yield

The weight hourly space velocity (WHSV) is defined as the ratio of the hourly feed flow rate of the ethanol and water mixture to the catalyst weight. This work presents the catalytic performances in terms of ethanol conversion (%), product selectivity (%), and product yield (%) based on molar carbon. The ethanol conversion was calculated as

$$X(\%) = \frac{n_{0_{EtOH}} - n_{1_{EtOH}}}{n_{0_{EtOH}}} \times 100 \quad (2)$$

where $n_{0_{EtOH}}$ is the number of moles fed into the reactor and $n_{1_{EtOH}}$ is the number of moles out of the reactor.

Selectivity is calculated by the following:

$$S_i\ (\%) = \frac{n_i \times c_i}{2\left(n_{0_{EtOH}} - n_{1_{EtOH}}\right)} \times 100 \quad (3)$$

where n_i is the number of moles of product i and c_i is the number of carbon atoms in product i (e.g., 1,3-BD is 4). The selectivity is given:

$$Y_i\ (\%) = S_i \times X \div 100 \quad (4)$$

The WHSV is defined as the ratio of the hourly feed flow rate of ethanol and the catalyst weight:

$$\text{WHSV } (\text{h}^{-1}) = \frac{\text{Flow rate of ethanol } \left(\frac{\text{g}}{\text{h}}\right)}{\text{mass of catalyst (g)}} \quad (5)$$

The following activity measures can be used for comparative measurements such as catalyst screening, process parameter determination, optimization of catalyst production conditions, and deactivation studies. Catalysts are frequently studied in constantly operating test reactors, where conversion rates at a constant space velocity are correlated. The volume flow rate V_0 concerning the catalyst mass m_{cat} is defined as the space velocity.

$$\text{Space Velocity} = \frac{v_o}{m_{cat}} \ (\text{m}^3\text{kg}^{-1}\text{s}^{-1}) \quad (6)$$

If the catalyst mass in Equation (5) is replaced with the catalyst volume, the space velocity is proportional to the reciprocal of the residence time. A reactor's performance is often given relative to the catalyst mass or volume so that reactors of different sizes or construction can be compared. This quantity is known as the space-time yield (STY):

$$\text{STY} = \frac{\text{Desired product quantity}}{\text{Catalyst volume} \cdot \text{time}} (\text{gkg}^{-1}\text{h}^{-1}) \quad (7)$$

3.4. Catalyst Characterization

The characterization of the catalyst was aided with XPS, XRD, and TGA. X-ray diffraction (XRD) patterns were acquired on a D2 phaser X-ray diffractometer, using monochromatic Cu Kα radiation and scanning 2θ from 10° to 90°, and operated at 40 kV and 40 mA using 0.1 g of the catalyst. The relative crystallinity is calculated according to the aggregate intensities of the three peaks at 2θ of different degrees of angles. X-ray diffraction analysis is an important basis for qualitative analysis of the catalyst. This analysis could identify surface crystallinity and catalyst type. It also aids the identification of peak position and signifies the characteristic properties of each catalyst. The catalytic surface chemistry was studied using X-ray photoelectron spectroscopy (XPS). The sample analysis was undertaken with the aid of 5700C (Perkin Elmer, Akron, OH, USA) model Physical and Electronics apparatus, with MgKα radiation (1253.6 eV) using 0.1 g of the catalyst. The available data fitting of the XPS peak was achieved using Gaussian squares or the Lorentzian peak geometry. For the catalytic chemical reaction of ethanol to butadiene, the thermal property of the catalyst after the reaction was analyzed using thermogravimetric (TGA) (TA instruments Q50, USA). This suggestion is important to identify the coke deposition on the catalyst. The sample was heated from 25 °C to 800 °C at a ramp rate of 10 °C/min under nitrogen gas flow conditions.

3.5. Catalyst Testing

For the generation of 1,3-butadiene from ethanol, a fixed bed reactor system was used under standard temperature and pressure. A sample of 0.4 g of the catalyst sample was packed in the middle of the stainless tube (R 1/4 22 mm) and inserted into the furnace. Using powered SiO_2 was induced to increase the bed length, allowing the flow condition. 0.4 g of catalyst was inserted into the fixed bed. Later, ethanol was induced with nitrogen gas with a 30 cm^3/min flow rate bubbling into saturated ethanol vapor, carried into the fixed bed reactor. The temperature of the bubbler was alternated by varying the WHSV (0.75 h^{-1}, 1.25 h^{-1}, 2.5 h^{-1}, and 6.0 h^{-1}). Before the chemical reaction, the catalyst was activated by heating to 400 °C. This suggestion was made to prevent both reactant and product condensation. This heating process was conducted at 15 °C/min and kept at 400 °C for 1 h under a 30 cm^3/min flow rate under nitrogen conditions. The main products (1,3-butadiene, ethylene, and acetaldehyde) were monitored using GC-14B, FID detector.

4. Conclusions

ZrO_2 combined with SiO_2 and CaO showed high catalytic activity and stable ethanol dehydration to 1,3-butadiene in terms of yield and selectivity. At WHSV of 2.5 h^{-1}, SiO_2-ZrO_2 has a selectivity of 94% of 1,3-butadiene at 350 °C and 14 h time on stream. 2% CaO-ZrO_2 has 90% selectivity of 1,3-butadiene at 350 °C and 12 h time on stream. When the reaction conditions were at WHSV of 1.25 h^{-1} and a temperature of 300 °C, the ethanol conversion was 87.9% for 10% SiO_2-ZrO_2 with a 79% yield and 85% selectivity of 1,3-butadiene. The 10% SiO_2-ZrO_2 catalyst shows no ethylene yield, as the catalytic reaction tends to forward the yield of 1,3-butadiene. The $Zr(OH)_2$ catalyst shows a low ethanol conversion at 14 h time on stream with a 20% ethanol conversion. $Zr(OH)_2$ exposed the basic nature of the Zr-containing catalyst, and for the yield of 1,3-butadiene to be realized, a catalyst should possess a balance between the acidic sites and Lewis sites.

The 2% CaO-ZrO_2 catalyst showed a low coke formation, which means it was more thermal stable than the rest, the order of thermal stability is as follows: 2% CaO-ZrO_2 > ZrO_2 > 10% SiO_2-ZrO_2 > $Zr(OH)_2$. XPS shows the carbon particle deposition in the catalyst affects the coke formation process, as $Zr(OH)_2$ has the highest carbon deposition (28.95%), hence the lowest stability. While 10% SiO_2-ZrO_2 has the lowest carbon deposition; hence, the highest instability and highest ethanol conversion.

Supplementary Materials: The following supporting information can be downloaded at: https://www.mdpi.com/article/10.3390/catal12070766/s1, Figure S1 Low-temperature N_2 adsorption-desorption curves. Figure S2 TGA curves of 50% CeO_2-ZrO_2 and 30% TiO_2-ZrO_2.

Author Contributions: Conceptualization, H.-S.W.; investigation, A.A.B.; writing—original draft preparation, A.A.B.; writing—review and editing, H.-S.W.; supervision, H.-S.W. All authors have read and agreed to the published version of the manuscript.

Funding: The ministry of science and technology of Taiwan: MOST 109-2221-E-155-009.

Institutional Review Board Statement: Not applicable.

Informed Consent Statement: Not applicable.

Data Availability Statement: No applicable.

Conflicts of Interest: The authors declare no conflict of interest.

References

1. Ochoa, J.V.; Bandinelli, C.; Vozniuk, O.; Chieregato, A.; Malmusi, A.; Recchi, C.; Cavani, F. An analysis of the chemical, physical and reactivity features of MgO–SiO_2 catalysts for butadiene synthesis with the Lebedev process. *Green Chem.* **2016**, *18*, 1653–1663. [CrossRef]
2. Talalay, A.; Talalay, L.S.K. The Russian synthetic rubber from alcohol. A survey of the chemistry and technology of the lebedev process for producing sodiumbutadiene polymers. *Rubber Chem. Technol.* **1942**, *15*, 403–429. [CrossRef]
3. Bhattacharyya, S.K.; Ganguly, N.D. One-step catalytic conversion of ethanol to butadiene in the fixed bed. I. Single-oxide catalysts. *J. Appl. Chem.* **1962**, *12*, 97–104. [CrossRef]
4. Boronat, M.; Concepción, P.; Corma, A.; Navarro, M.T.; Renz, M.; Valencia, S. Reactivity in the confined spaces of zeolites: The interplay between spectroscopy and theory to develop structure–activity relationships for catalysis. *Phys. Chem. Chem. Phys.* **2009**, *11*, 2876–2884. [CrossRef]
5. Boronat, M.; Concepción, P.; Corma, A.; Renz, M.; Valencia, S. Determination of the catalytically active oxida-tion Lewis acid sites in Sn-beta zeolites, and their optimisation by the combination of theoretical and experimental studies. *J. Catal.* **2005**, *234*, 111–118. [CrossRef]
6. Boukha, Z.; Fitian, L.; López-Haro, M.; Mora, M.; Ruiz, J.R.; Jiménez-Sanchidrián, C.; Blanco, G.; Calvino, J.J.; Cifredo, G.A.; Trasobares, S.; et al. Influence of the calcination temperature on the nano-structural properties, surface basicity, and catalytic behavior of alumina-supported lanthana samples. *J. Catal.* **2010**, *272*, 121–130. [CrossRef]
7. Cabello González, G.M.; Villanueva Perales, A.L.; Martínez, A.; Campoy, M.; Vidal-Barrero, F. Conversion of aqueous ethanol/acetaldehyde mixtures into 1,3-butadiene over a mesostructured Ta-SBA-15 catalyst: Effect of reaction conditions and kinetic modelling. *Fuel Process. Technol.* **2022**, *226*, 107092. [CrossRef]
8. Aimon, D.; Panier, E. La mise en pratique de l'économie circulaire chez michelin. *Ann. Mines-Responsab. Environ.* **2014**, *76*, 38–44. [CrossRef]

9. Budagumpi, S.; Kim, K.-H.; Kim, I. Catalytic and coordination facets of single-site non-metallocene organometallic catalysts with N-heterocyclic scaffolds employed in olefin polymerization. *Coord. Chem. Rev.* **2011**, *255*, 2785–2809. [CrossRef]
10. Prillaman, J.T.; Miyake, N.; Davis, R.J. Calcium Phosphate Catalysts for Ethanol Coupling to Butanol and Butadiene. *Catal. Lett.* **2020**, *151*, 648–657. [CrossRef]
11. Pomalaza, G.; Arango, P.; Capron, M.; Dumeignil, F.Y. Ethanol-to-Butadiene: A Review. *Catal. Sci. Technol.* **2020**, *10*, 4860–4911. [CrossRef]
12. Gao, M.; Jiang, H.; Zhang, M. Influences of Interactive Effect Between ZrO_2 and nano-SiO_2 on the formation of 1,3-butadiene from ethanol and acetaldehyde. *Catal. Surv. Asia* **2020**, *24*, 115–122. [CrossRef]
13. Zhang, M.; Guan, X.; Zhuang, J.; Yu, Y. Insights into the mechanism of ethanol conversion into 1,3-butadiene on Zr-β zeolite. *Appl. Surf. Sci.* **2021**, *579*, 152212. [CrossRef]
14. Kyriienko, P.I.; Larina, O.V.; Balakin, D.Y.; Vorokhta, M.; Khalakhan, I.; Sergiienko, S.A.; Soloviev, S.O.; Orlyk, S.M. The effect of lanthanum in Cu/La(-Zr)-Si oxide catalysts for aqueous ethanol conversion into 1,3-butadiene. *Mol. Catal.* **2022**, *518*, 112096. [CrossRef]
15. Sushkevich, V.L.; Ivanova, I.I. Ag-Promoted ZrBEA Zeolites Obtained by Post-Synthetic Modification for Conversion of Ethanol to Butadiene. *ChemSusChem* **2016**, *9*, 2216–2225. [CrossRef]
16. Sushkevich, V.L.; Ivanova, I.I.; Ordomsky, V.V.; Taarning, E. Design of a metal-promoted oxide catalyst for the selective synthesis of butadiene from ethanol. *ChemSusChem* **2014**, *7*, 2527–2536. [CrossRef]
17. Kyriienko, P.I.; Larina, O.V.; Balakin, D.Y.; Stetsuk, A.O.; Nychiporuk, Y.M.; Soloviev, S.O.; Orlyk, S.M. 1,3-Butadiene production from aqueous ethanol over ZnO/MgO-SiO_2 catalysts: Insight into H_2O effect on catalytic performance. *Appl. Catal. A Gen.* **2021**, *616*, 118081. [CrossRef]
18. Cheong, J.L.; Shao, Y.; Tan, S.J.R.; Li, X.; Zhang, Y.; Lee, S.S. Highly Active and Selective Zr/MCF Catalyst for Production of 1,3-Butadiene from Ethanol in a Dual Fixed Bed Reactor System. *ACS Sustain. Chem. Eng.* **2016**, *4*, 4887–4894. [CrossRef]
19. Pomalaza, G.; Capron, M.; Ordomsky, V.; Dumeignil, F. Recent breakthroughs in the conversion of ethanol to butadiene. *Catalysts* **2016**, *6*, 203. [CrossRef]
20. Guan, Y.; Hensen, E.J.M. Ethanol dehydrogenation by gold catalysts: The effect of the gold particle size and the presence of oxygen. *Appl. Catal. A Gen.* **2009**, *361*, 49–56. [CrossRef]
21. Han, Z.; Li, X.; Zhang, M.; Liu, Z.; Gao, M. Sol–gel synthesis of ZrO_2–SiO_2 catalysts for the transformation of bioethanol and acetaldehyde into 1,3-butadiene. *RSC Adv.* **2015**, *5*, 103982–103988. [CrossRef]
22. Baylon, R.A.L.; Sun, J.; Wang, Y. Conversion of ethanol to 1,3-butadiene over Na doped ZnxZryOz mixed metal oxides. *Catal. Today* **2016**, *259*, 446–452. [CrossRef]
23. Kuznetsov, P.; Belskaya, N.A.; Tomilova, T.A.; Beregovtsova, N.G.; Sharypov, V. Peculiarities in methanol action during liquefaction of different coal type. *Fuel* **1989**, *68*, 1580–1583. [CrossRef]
24. Kongwudthiti, S.; Praserthdam, P.; Tanakulrungsank, W.; Inoue, M. The influence of Si–O–Zr bonds on the crys-tal-growth inhibition of zirconia prepared by the glycothermal method. *J. Mater. Process. Technol.* **2003**, *136*, 186–189. [CrossRef]
25. Feng, X.-J.; Lu, X.-B.; He, R. Tertiary amino group covalently bonded to MCM-41 silica as heterogeneous cata-lyst for the continuous synthesis of dimethyl carbonate from methanol and ethylene carbonate. *Appl. Catal. A Gen.* **2004**, *272*, 347–352. [CrossRef]
26. Zou, H.; Lin, Y. Structural and surface chemical properties of sol–gel derived TiO_2–ZrO_2 oxides. *Appl. Catal. A Gen.* **2004**, *265*, 35–42. [CrossRef]
27. Suda, A.; Yamamura, K.; Morikawa, A.; Nagai, Y.; Sobukawa, H.; Ukyo, Y.; Shinjo, H. Atmospheric pressure sol-vothermal synthesis of ceria–zirconia solid solutions and their large oxygen storage capacity. *J. Mater. Sci.* **2008**, *43*, 2258–2262. [CrossRef]
28. Chen, Z.; Zhang, X.; Yang, F.; Peng, H.; Zhang, X.; Zhu, S.; Che, L. Deactivation of a Y-zeolite based catalyst with coke evolution during the catalytic pyrolysis of polyethylene for fuel oil. *Appl. Catal. A Gen.* **2021**, *609*, 117873. [CrossRef]
29. Zhang, M.; Qin, Y.; Jiang, H.; Wang, L. Protective desilication of β zeolite: A mechanism study and its applica-tion in ethanol-acetaldehyde to 1, 3-butadiene. *Microporous Mesoporous Mater.* **2021**, *326*, 111359. [CrossRef]
30. Wu, C.-Y.; Wu, H.-S. Ethylene formation from ethanol dehydration using ZSM-5 catalyst. *ACS Omega* **2017**, *2*, 4287–4296. [CrossRef]
31. Sekiguchi, Y.; Akiyama, S.; Urakawa, W.; Koyama, T.r.; Miyaji, A.; Motokura, K.; Baba, T. One-step catalytic conversion of ethanol into 1,3-butadiene using zinc-containing talc. *Catal. Commun.* **2015**, *68*, 20–24. [CrossRef]
32. Jones, M.D.; Keir, C.G.; Di Iulio, C.; Robertson, R.A.; Williams, C.V.; Apperley, D.C. Investigations into the con-version of ethanol into 1, 3-butadiene. *Catal. Sci. Technol.* **2011**, *1*, 267–272. [CrossRef]
33. Lesmana, D.; Wu, H.-S. Modified oxalic acid co-precipitation method for preparing Cu/ZnO/Al_2O_3/Cr_2O_3/CeO_2 catalysts for the OR (oxidative reforming) of M (methanol) to produce H2 (hydrogen) gas. *Energy* **2014**, *69*, 769–777. [CrossRef]